2016 IEEE Intelligent Vehicles Symposium (IV)
Gothenburg, Sweden, June 19-22, 2016

Experimental Validation of Geometric Path Following Control with Demand Supervision on an Over-Actuated Robotic Vehicle

Peter Ritzer, Christoph Winter and Jonathan Brembeck

Abstract—**This work describes the development and experimental validation of a geometric path following control strategy with demand supervision applied to an over-actuated robotic vehicle, the ROboMObil [1]. The proposed method enables the ROboMObil to automatically follow paths while the driver is free to control the velocity along the path. Beside the longitudinal degree of freedom, two lateral degrees of freedom can be controlled relative to the path. If this demand interface were provided without supervision, the driver may potentially overwrite the path following control in a manner such that the vehicle limits are violated and the vehicle becomes unstable. To avoid such critical situations a demand supervisor is introduced into the path following framework. The work concludes by a simulative demonstration of the supervised control system and an experimental validation of the presented approach implemented in the ROboMObil.**

I. Introduction

Path following control is one of the central motion control problems which have to be solved for the development of autonomous vehicles. Much research has been done on this topic considering the control of conventional vehicles. In [2] a time domain closed loop controller based on a single track model is employed for lateral path following of an autonomous vehicle. Additionally [2] proposes a steering angle offset observer to compensate model inaccuracies. Also in [3] a time domain control based on a front steered single track model is proposed for lane keeping. In this approach the vehicle velocity is used as model parameter such that the applied controller pole placement requires time variant poles. The control variables employed in the controller are lateral displacement and orientation offset. However, only the desired lateral displacement to the path can be set by the user, due to the limited degrees of freedom of the considered vehicle architecture. In [4] a cost function based path following control approach is proposed to solve the allocation between orientation and displacement demand. This approach predicts the vehicle behavior for a certain time period and finds the best trade-off between orientation and lateral offset. Finally in [5] a time independent path following controller for a conventional car is discussed which expresses the controller dynamics in dependence of the planned path's arc length.

This paper uses the experience learned from literature and the previous work in [6] to further develop the centralized control approach for the automatic driving of an overactuated robotic vehicle. While the work in [6] studies the feasibility of a time domain control approach combined with an *optimization based control allocation* (OCA), this work transfers the time independent approach of [5] to the overactuated ROboMObil case. The main focus is to enable the experimental validation of the path following control and its application as shared autonomy demonstrator. For this purpose, the *path following controller* (PFC) is redesigned as *geometric* PFC (geoPFC) approach to meet the reliability requirements and a demand supervisor is developed to enable a secure control of the vehicle in path following mode.

The first step to ensure this requirement is a change in the controller architecture of [6]. Since the numerical stability of the optimization routine in the OCA is not guaranteed it is replaced by the well tested *geometric control based allocation* (GCA) method described in [7]. The GCA relies on the extension of Ackermann steering on a four wheel steer vehicle and the assumption of zero wheel slip. Hence it is simple but produces inaccuracies in driving situations with high wheel slip. The simplicity is of great value for the considered application since it enables a valid mapping to be guaranteed for all driving situations. On the other hand, the inaccuracies in extreme driving situations are not disadvantageous for this application since these situations are usually avoided through the demanded path and limited user demand range. Furthermore, it is possible to extend the GCA as shown in [8] with closed loop control to compensate for excessive slip values. The interface of the GCA is different to that of the OCA such that a further adaption of the former path following algorithm of [6] is necessary. The details of this step are discussed in Section IV.

The second step in the design of a safe geoPFC is the online validation of the user demands through a demand supervisor. In contrast to the algorithms in [3] or [4] the geoPFC of the ROboMObil allows to set lateral displacement and orientation offset independently. Hence, the difficulty is not to find a tradeoff between these two demands, but to provide a new functionality of the geoPFC which supervises the lateral demands such that the four independent steering angle constraints of the ROboMObil are not violated. The details of the lateral user demand supervisor are explained in Section V.

Peter Ritzer is research assistant in the Automotive Vehicle System Dynamics Department in the DLR Institute of System Dynamics and Control, Oberpfaffenhofen, Germany. (Peter.Ritzer@dlr.de)
Christoph Winter is research assistant in the Automotive Vehicle System Dynamics Department in the DLR Institute of System Dynamics and Control, Oberpfaffenhofen, Germany. (Christoph.Winter@dlr.de)
Jonathan Brembeck is head of the Automotive Vehicle System Dynamics Department in the DLR Institute of System Dynamics and Control, Oberpfaffenhofen, Germany. (Jonathan.Brembeck@dlr.de)

II. Notation

For the efficient notation of the presented algorithms, different coordinate systems are used. Fig. 1 exemplarily shows the different frames denoted by the superscript I, C and P for Inertial, Car and Path frame, respectively. The affiliation of the signal to the Car or the Path is denoted by subscripts C or P.

III. Motion Demand And Feedback

A. Demand representation

The employed demand representation is formulated as in [6] and repeated here for the sake of completeness. The motion demand $\boldsymbol{\lambda}(s)$ of the geoPFC is a generalized path with respect to its arc length s. The elements of the parametric curve $\boldsymbol{\lambda}(s) \in \mathbb{R}^5$ are illustrated in Fig. 1. They encompass the demanded path position, a plane curve $\boldsymbol{p}_{\mathrm{P}}^{\mathrm{I}}(s) \in \mathbb{R}^2$, path orientation $\psi_{\mathrm{P}}(s)$ and path curvature $\kappa_{\mathrm{P}}(s)$. In addition the maximal vehicle velocity $v_x^{\mathrm{P}}(s)$ along the path tangent $\boldsymbol{x}^{\mathrm{P}}$ is part of the motion demand. Noteworthy is that the partial derivatives $\frac{\mathrm{d}}{\mathrm{d}s}\boldsymbol{p}_{\mathrm{P}}^{\mathrm{I}}(s)$ and $\frac{\mathrm{d}}{\mathrm{d}s}\psi_{\mathrm{P}}(s)$ are implicitly part of the motion demand

$$\frac{\mathrm{d}}{\mathrm{d}s}\boldsymbol{p}_{\mathrm{P}}^{\mathrm{I}}(s) = (\cos\psi_{\mathrm{P}}(s) \quad \sin\psi_{\mathrm{P}}(s))^T \tag{1}$$

$$\frac{\mathrm{d}}{\mathrm{d}s}\psi_{\mathrm{P}}(s) = \kappa_{\mathrm{P}}(s)\,. \tag{2}$$

These partial derivatives are necessary for the geometric path following control in Section IV and the online calculation of the user demand limits in Section V. The definition of motion demands in this form has the advantage that it enables geometric path planning as proposed in [9]. This method allows position, orientation and velocity demands to be defined independently of time and therefore the motion demand can be calculated offline as a function of arc length s. As a general interface to path planning modules the motion demand $\boldsymbol{\lambda}(s)$ is represented as look-up table.

B. Feedback calculation

The demanded path in the motion demand representation and the control algorithm are expressed in the horizontal plane $\mathbb{R}^2$. In a real world application the position measurements collected via a dGPS sensor are a spatial curve. However, the processing of these signals in the controller requires expressing both signals in the same space. Since the control algorithm is expressed in $\mathbb{R}^2$ the reasonable approach is to map the measured spatial curve to a plane curve in $\mathbb{R}^2$. A first step is to use only the latitude and longitude information of the dGPS sensor, which projects the measured path to a spherical curve. In a second step, these spherical positions are converted into positions in a fixed inertial frame. The frame is defined as a tangent space to the earth which is a plane Cartesian system with $\boldsymbol{x}^{\mathrm{I}}$ and $\boldsymbol{y}^{\mathrm{I}}$ axis. It is defined by the GPS coordinates (ϕ_0, θ_0) of its origin and the orientation ψ^{world} as the angle between east direction and the $\boldsymbol{x}^{\mathrm{I}}$-axis. Using this plane coordinate system in the PFC simplifies the calculation of control errors and feed forward control inputs. A drawback of this simplification is the resulting presence of deviations between demanded and driven path rooted in the curvature and slope of the earth. Nevertheless, these effects are not relevant for vehicle operations in vicinity of the origin, which is the case for the application as shared autonomy demonstrator but also for future applications where an online planning algorithm is imaginable which is cyclically setting up the demanded path relative to a variable inertial system origin.

IV. Geometric Path Following Control

A. Motivation of the geometric approach

The PFC described in the following is extending the algorithm presented in [6]. The extension is tailored for the use of the GCA implemented on the ROboMObil. The GCA is an allocation method combining a geometrical approach for the allocation of the steering demands and an even distribution of the wheel torques. The interface of the GCA covers the planar degrees of freedom of the ROboMObil in the form of the absolute vehicle velocity v_{C}, the side slip angle of the vehicle β and the instantaneous center of rotation (ICR) curvature ρ_{ICR}. This is a velocity interface with the lateral demands represented independent of the vehicle velocity as normalized demands. The advantage of this interface is that the steering angle allocation is valid at any speed

$$\beta = \operatorname{atan}\left(\frac{v_{\mathrm{C}y}^{\mathrm{C}}}{v_{\mathrm{C}x}^{\mathrm{C}}}\right) \tag{3}$$

$$\rho_{\mathrm{ICR}} = \frac{\dot{\psi}_{\mathrm{C}}}{v_{\mathrm{C}}}. \tag{4}$$

In contrast to the GCA the OCA provides an acceleration interface such that a direct adoption of the PFC algorithm of [6] is not possible. In a first adaption step of the PFC for the GCA interface it was recognized that a reformulation of the controller for velocity demands $v_{\mathrm{C}x}^{\mathrm{C}*}$, $v_{\mathrm{C}y}^{\mathrm{C}*}$, $\dot{\psi}_{\mathrm{C}}^{*}$ and a subsequent conversion of the demands to the GCA interface is only feasible for vehicle speeds above some low speed threshold. This is due to the noise in the speed measurements and the necessary normalizations in (3) and (4). For vehicle motions with speed lower than this threshold, especially stopping maneuvers, a control mode switching to an open loop path following approach is necessary. With this extension it is possible to use the algorithm in practice. However, this approach is not satisfactory since it sacrifices the stability of the PFC in low speed operation through disabling the feedback and produces random steering command fluctuations due to the noise amplification in the demand normalization.

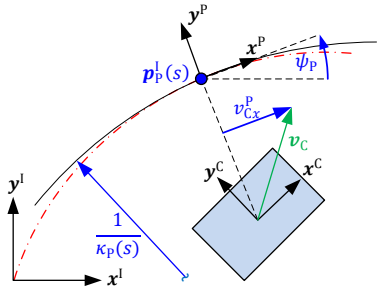

Fig. 1: Geometric quantities and reference control variables defining the motion demand $\boldsymbol{\lambda}(s)$.

To overcome these difficulties it is necessary to scale the controller and input filter dynamics with vehicle speed and exchange time with arc length as independent variable in the differential equations as proposed in [10]. Using this method the designed controller is reacting slower for lower speeds and is stopped for zero speed. Furthermore it allows the direct incorporation of the lateral GCA interface variables β and ρ_{ICR} into the controller design which makes the conversions (3) and (4) obsolete. With these measures applied to the lateral control channels while keeping the longitudinal control of the vehicle in time domain yields the geoPFC Algorithm.

B. Geometric Path Following Control Algorithm

In the first step of the lateral controller design the desired system behavior is defined for a generic variable x. Starting from equation (5) which describes the desired control error dynamics as a first order system in time domain and applying the normalization of this differential equation

$$\frac{\mathrm{d}x - \mathrm{d}x^*}{\mathrm{d}t} = -\frac{x - x^*}{\tau_x} \tag{5}$$

with the absolute vehicle speed

$$v_{\mathrm{C}} = \frac{\mathrm{d}q}{\mathrm{d}t} \tag{6}$$

a path domain formulation of (5) results in (7). This transformation proposed in [10], results in replacing time t by the arc length of the vehicle path q (not to be confused with the arc length of the demanded path s, which is used in [5], parameterizing the motion demand in III.A) and the time constant τ_x by the path constant λ_x

$$\frac{\mathrm{d}x - \mathrm{d}x^*}{\mathrm{d}q} = -\frac{x - x^*}{\lambda_x}. \tag{7}$$

This generic equation defines the desired speed normalized first order behavior of the lateral control errors in the geoPFC. Substituting x by the orientation offset $\Delta\psi$ and the lateral displacement $e_{\mathrm{y}}^{\mathrm{P}}$ yields the desired dynamics of the geoPFC lateral commands

$$\frac{\mathrm{d}\Delta\psi}{\mathrm{d}q} = \frac{\mathrm{d}\Delta\psi^*}{\mathrm{d}q} - \frac{(\Delta\psi - \Delta\psi^*)}{\lambda_\psi} \tag{8}$$

$$\frac{\mathrm{d}e_{\mathrm{y}}^{\mathrm{P}}}{\mathrm{d}q} = \frac{\mathrm{d}e_{\mathrm{y}}^{\mathrm{P*}}}{\mathrm{d}q} - \frac{e_{\mathrm{y}}^{\mathrm{P}} - e_{\mathrm{y}}^{\mathrm{P*}}}{\lambda_e}. \tag{9}$$

Here λ_e and λ_ψ are the path constants, representing the path distance after which the control errors are reduced to 37 % of the initial error. Hence, λ_e and λ_ψ are parameters to characterize the reaction "speed" of the control law independently of time.

In the second step of the controller design, the derivatives of the control variable in (8) and (9) are related to the lateral GCA inputs side slip angle β^* and the so called instantaneous center of rotation curvature ρ_{ICR}^*.

The orientation offset derivative $\frac{\mathrm{d}\Delta\psi}{\mathrm{d}q}$ is

$$\frac{\mathrm{d}\Delta\psi}{\mathrm{d}q} = \kappa_{\mathrm{P}}\frac{\mathrm{d}s}{\mathrm{d}q} - \rho_{\mathrm{ICR}}^* \tag{10}$$

using the definitions of

$$\rho_{\mathrm{ICR}}^* = \frac{\mathrm{d}\psi_{\mathrm{C}}}{\mathrm{d}q} \tag{11}$$

$$\kappa_{\mathrm{P}} = \frac{\mathrm{d}\psi_{\mathrm{P}}}{\mathrm{d}s} \tag{12}$$

and

$$\Delta\psi = \psi_{\mathrm{P}} - \psi_{\mathrm{C}}\,. \tag{13}$$

The calculation of the lateral displacement derivative $\frac{\mathrm{d}e_{\mathrm{y}}^{\mathrm{P}}}{\mathrm{d}q}$ requires the computation of the Jacobian matrix $J_{e_{\mathrm{y}}^{\mathrm{P}}}(\psi_{\mathrm{P}}, x_{\mathrm{C}}^{\mathrm{I}}, y_{\mathrm{C}}^{\mathrm{I}}, x_{\mathrm{P}}^{\mathrm{I}}, y_{\mathrm{P}}^{\mathrm{I}})$ of the lateral displacement $\mathrm{e}_y^{\mathrm{P}}$, given by

$$\mathrm{e}_y^{\mathrm{P}} = -\sin(\psi_{\mathrm{P}})\left(x_{\mathrm{P}}^{\mathrm{I}} - x_{\mathrm{C}}^{\mathrm{I}}\right) + \cos(\psi_{\mathrm{P}})\left(y_{\mathrm{P}}^{\mathrm{I}} - y_{\mathrm{C}}^{\mathrm{I}}\right). \tag{14}$$

With this Jacobian, (12) and the derivatives defined in (17) - (20), the path derivative of the lateral displacement can be expressed as

$$\frac{\mathrm{d}e_y^{\mathrm{P}}}{\mathrm{d}q} = J_{e_{\mathrm{y}}^{\mathrm{P}}} \cdot \begin{pmatrix} \frac{\mathrm{d}\psi_P}{\mathrm{d}q} & \frac{\mathrm{d}x_{\mathrm{C}}^{\mathrm{I}}}{\mathrm{d}q} & \frac{\mathrm{d}y_{\mathrm{C}}^{\mathrm{I}}}{\mathrm{d}q} & \frac{\mathrm{d}x_{\mathrm{P}}^{\mathrm{I}}}{\mathrm{d}q} & \frac{\mathrm{d}y_{\mathrm{P}}^{\mathrm{I}}}{\mathrm{d}q} \end{pmatrix}^T \tag{15}$$

which can be simplified to

$$\frac{\mathrm{d}e_y^{\mathrm{P}}}{\mathrm{d}q} = \frac{\mathrm{d}s}{\mathrm{d}q}\,\kappa_{\mathrm{P}} e_x^{\mathrm{P}} - \sin(\beta^* - \Delta\psi). \tag{16}$$

In this equation e_x^{P} is the tangential component of the position error $\boldsymbol{e} = \boldsymbol{p}_{\mathrm{P}}^{\mathrm{I}} - \boldsymbol{p}_{\mathrm{C}}^{\mathrm{I}}$ in the path frame introduced in the Time Independent Path Interpolator in [6]

$$\frac{\mathrm{d}x_{\mathrm{C}}^{\mathrm{I}}}{\mathrm{d}q} = \cos(\beta^* + \psi_{\mathrm{C}}) \tag{17}$$

$$\frac{\mathrm{d}y_{\mathrm{C}}^{\mathrm{I}}}{\mathrm{d}q} = \sin(\beta^* + \psi_{\mathrm{C}}) \tag{18}$$

$$\frac{\mathrm{d}x_{\mathrm{P}}^{\mathrm{I}}}{\mathrm{d}q} = \cos(\psi_P)\frac{\mathrm{d}s}{\mathrm{d}q} \tag{19}$$

$$\frac{\mathrm{d}y_{\mathrm{P}}^{\mathrm{I}}}{\mathrm{d}q} = \sin(\psi_P)\frac{\mathrm{d}s}{\mathrm{d}q}. \tag{20}$$

In the final step of the lateral control design the equation system set up by equating the control demand dynamics in (8) and (9) to the respective counterpart (10) and (16) has to be solved for β^* and ρ_{ICR}^*. Equation (10) and (16) show that $\frac{\mathrm{d}\Delta\psi}{\mathrm{d}q}$ and $\frac{\mathrm{d}e_{\mathrm{y}}^{\mathrm{P}}}{\mathrm{d}q}$ both depend on the curvature κ_{P} of the planned path and the ratio of the demanded path arc length increment to the real vehicle arc length increment $\frac{\mathrm{d}s}{\mathrm{d}q}$. Since the curvature κ_{P} is known, no coupling between (10) and (16) is introduced through this variable. However, using the estimate of the path parameter rate $\hat{\dot{s}} = \frac{\mathrm{d}s}{\mathrm{d}t}$ derived in [6] and the definition of the tangential vehicle velocity

$$v_{\mathrm{C}x}^{\mathrm{P}} = \cos(\beta^* - \Delta\psi)\frac{\mathrm{d}q}{\mathrm{d}t} \tag{21}$$

it can be shown that the ratio $\frac{\mathrm{d}s}{\mathrm{d}q}$ depends on the unknown variable β^*.

This dependency introduces a coupling between (10) and (16) which can be solved by first solving for β^* and then using this solution to solve for ρ_{ICR}^*.

The equation (9) equal (16) can be reformulated into

$$0 = a + b \cdot \cos(\xi) + \sin(\xi) \tag{22}$$

using the substitutions

$$a = \frac{\mathrm{d}e_y^{\mathrm{P}*}}{\mathrm{d}q} - \frac{e_y^{\mathrm{P}} - e_y^{\mathrm{P}*}}{\lambda_e} \tag{23}$$

$$b = \frac{\kappa_{\mathrm{P}} e_x^{\mathrm{P}}}{e_y^{\mathrm{P}} \kappa_{\mathrm{P}} + 1} \tag{24}$$

$$\xi = \beta^* - \Delta\psi\,. \tag{25}$$

The result in (22) can be solved analytically for two solutions of ξ. Selecting the suitable solution and using (25) then yields the side slip angle demand.

Now the lateral geoPFC feedback control law can be described by (26) and (27), with i the imaginary unit and ln() the natural logarithm

$$\beta^* = -\ln\left(-\frac{a + \sqrt{a^2 - b^2 - 1}}{b - i}\right) \cdot i + \Delta\psi. \tag{26}$$

Knowing β^* it is straightforward to calculate ρ_{ICR}^*

$$\rho_{\mathrm{ICR}}^* = \frac{\Delta\psi - \Delta\psi^*}{\lambda_\psi} - \frac{\mathrm{d}\Delta\psi^*}{\mathrm{d}q} + \kappa_{\mathrm{P}} \frac{\cos(\beta^* - \Delta\psi)}{e_y^{\mathrm{P}} \kappa_{\mathrm{P}} + 1}. \tag{27}$$

The longitudinal control channel of the geoPFC requires no feedback control. The GCA already implements a longitudinal velocity interface through a cascade of acceleration and velocity controller such that only the velocity demand limitation and filtering, discussed in the following section, is necessary to produce feasible demands.

In the case of the lateral control channel, the demand filtering and supervision is more complex, compared to that of the longitudinal channel. Hence, the filtering and saturation strategies are introduced separately. The control input filtering method, needed for the calculation of the path derivatives of the user demands, is outlined in Section IV.D. The adaptive demand limitation, necessary to sustain the feasibility of the path following task in all driving situations, is introduced in Section V.

C. Velocity demand limitation and filtering

Although the GCA interface provides a longitudinal velocity interface the geoPFC provides velocity and acceleration input modes to the driver. In the velocity mode the driver input u_v directly represents $v_{Cx}^{\mathrm{P}*}$, which is then limited to $\bar{v}_{Cx}^{P}$ and subsequently filtered. The filter used is a time domain first order lag element with rate limitation. The $\mathrm{sat}(u, \underline{u}, \bar{u})$ function used in (28) limits the acceleration to the range between lower $\underline{\dot{v}}_{Cx}^{\mathrm{P}}$ and upper $\bar{\dot{v}}_{Cx}^{\mathrm{P}}$ acceleration limits

$$\dot{v}_{Cx}^{\mathrm{P}*} = \mathrm{sat}\left(\frac{1}{\tau_v}\left(u_v - v_{Cx}^{\mathrm{P}*}\right), \underline{\dot{v}}_{Cx}^{\mathrm{P}}, \bar{\dot{v}}_{Cx}^{\mathrm{P}}\right). \tag{28}$$

In case the acceleration mode is active the user demand is considered as $\dot{v}_{Cx}^{\mathrm{P}*}$ which is integrated such that the velocity and acceleration limits are observed.

The acceleration limits $\bar{\dot{v}}_{Cx}^{\mathrm{P}}$ and $\underline{\dot{v}}_{Cx}^{\mathrm{P}}$ used in this filter and integrator represent the traction and braking torque limits of the ROboMObil, and therefore they stay constant apart from their dependency of the driving direction. The velocity limit $\bar{v}_{Cx}^{P}$ is intended to limit the lateral acceleration when the vehicle is driving in corners. Hence, the velocity limit is depending on the maximum acceptable lateral acceleration $\bar{a}_{\mathrm{lat}}$ and the current curve radius r_{C}

$$\bar{v}_{Cx}^{\mathrm{P}} = \sqrt{\bar{a}_{\mathrm{lat}} r_{\mathrm{C}}}\,. \tag{29}$$

The curve radius depends on the demanded path curvature κ_{P} and the measured lateral displacement e_y^{P}

$$r_{\mathrm{C}} = \left|\frac{1}{\kappa_{\mathrm{P}}} + e_y^{\mathrm{P}}\right|. \tag{30}$$

In practice it is preferable to saturate the vehicle velocity before reaching the curve. In the experimental setup, this is achieved by using the unfiltered demanded value of the lateral displacement $e_y^{\mathrm{P}*}$ and a preview value of κ_{P} which is the maximum absolute curvature within a speed dependent window.

D. Lateral Control Input Filtering

The control laws in (26) and (27) require the calculation of the path derivatives of the driver demands $\frac{\mathrm{d}e_y^{\mathrm{P}*}}{\mathrm{d}q}$ and $\frac{\mathrm{d}\Delta\psi^*}{\mathrm{d}q}$. For this purpose, the driver demand values are filtered by first order lag elements, expressed in path domain. This means that with the same transformation employed in the controller design, the differential equations of the demand filters are expressed in dependence of arc length q. Using the transformation yields the generic continuous filter equation

$$\frac{\mathrm{d}y}{\mathrm{d}q} = \frac{1}{\lambda_y}(u - y), \tag{31}$$

with u the filter input and y the filter output. The path constant λ_y defines the dynamics of the filter. Based on equation (31), the implemented filter is derived applying zero order hold discretization in path domain. Using the path increment $\Delta q = v \cdot T_{\mathrm{S}}$ analogously to the sampling time T_{S} in a time domain filter yields the difference equation of the demand filter with time step k

$$y_{[k+1]} = \Delta q_{[k]} \underbrace{\frac{1}{\lambda_y}\left(u_{[k]} - y_{[k]}\right)}_{\frac{\mathrm{d}y}{\mathrm{d}q}_{[k]}} + y_{[k]}. \tag{32}$$

Applying this filter on the user demand for the lateral control variables, allows the use of (31) for the calculation of the demand signal derivative employed in the control law.

An extension of the demand filter in (32) allows the incorporation of rate limitation of the respective demand

$$y_{[k+1]} = \mathrm{sat}\left(\Delta y_{[k]}, \underline{\frac{\mathrm{d}y}{\mathrm{d}q}} \Delta q_{[k]}, \overline{\frac{\mathrm{d}y}{\mathrm{d}q}} \Delta q_{[k]}\right) + y_{[k]}. \tag{33}$$

In the rate limited case the calculation of the demand derivative is

$$\frac{\mathrm{d}y}{\mathrm{d}q}_{[k]} = \frac{\mathrm{sat}\left(\Delta y_{[k]}, \underline{\frac{\mathrm{d}y}{\mathrm{d}q}} \Delta q_{[k]}, \overline{\frac{\mathrm{d}y}{\mathrm{d}q}} \Delta q_{[k]}\right)}{\Delta q_{[k]}}. \tag{34}$$

The demand filters used in the lateral control channel of the geoPFC are second order filters created by cascading two of the introduced filters. For the $\Delta\psi^*$ channel two filters

according to (32) are used and for the e_y^* channel filter (32) is combined in series with filter (33).

V. Lateral User Demand Supervisor

In addition to demand filtering, which serves to smooth the user inputs, it is necessary to incorporate adaptive limits for the lateral demands e_y^{P}, $\Delta\psi$ and the derivative $\frac{\mathrm{d}e_y^{\mathrm{P}}}{\mathrm{d}q}$ to sustain control feasibility in all driving situations.

A. Motivation for online adaption of lateral user demands

The motivation for the online adaption of the user demands is the aim of fully exploiting the steering angle range of the ROboMObil while guaranteeing the feasibility of the driver demands and the path following task. An example of the vehicle behavior without considering the steering angle limitations at the driver demand level is given in Fig. 2. In this experiment the ROboMObil negotiates a U-Turn while the driver demands an orientation offset $\Delta\psi$ of 10 degrees. The U-Turn together with the orientation offset demand requires steering angles beyond the limits. Since the driver demand is not limited the steering angle limitation forces the vehicle to depart from the path with a peak lateral displacement of one meter.

This behavior probably is unexpected to the driver and leads to confusion. More intuitive would be that the driver demands are reduced in order to keep the primary geoPFC path following task feasible. This motivates the introduction of a demand supervisor. To achieve this, supervisors based on pseudo control hedging [11] were investigated. However, simulative investigations show that the saturation based driver demand adaption, outlined in Fig. 3 and explained in detail in the following sections, shows better performance and stability for the use-case discussed here.

B. Driver demand supervisor overview

The basic idea of the supervisor design is to calculate the feasible driver demand ranges based on a geometric vehicle model, the preplanned path and the driver demands. With this exclusive use of feedforward variables it is possible to formulate the supervisor in the form of a feedforward filter which is not part of the control loop. This architecture assures that the stability properties of the geoPFC control loop are not affected.

A sequenced approach which introduces a prioritization of the lateral displacement demand over the orientation offset demand is used to compute the limits employed in the saturation based supervisor. The effect of this prioritization is that the orientation offset demand is reduced primarily

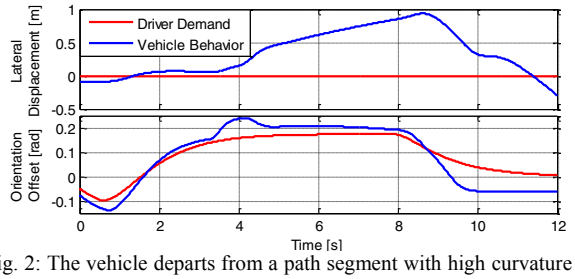

Fig. 2: The vehicle departs from a path segment with high curvature due to an infeasible orientation offset demand which requires steering angles beyond the mechanical limits.

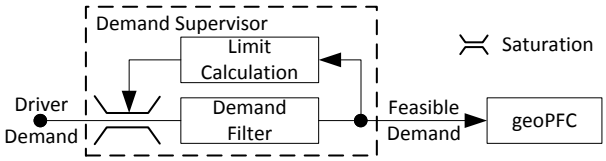

Fig. 3: Saturation based driver demand adaption.

while the lateral displacement demand is fully maintained. If this reduction is not sufficient to meet the steering angle limits then also the lateral displacement demand is reduced.

C. Saturation based supervisor

In Section IV.D the basic filter algorithm for the input smoothing and the calculation of the demand derivatives is described. In this section this filter is extended to a driver demand supervisor with the aim to reduce the occurrence of saturated steering angles. For this purpose, the first order filters at the end of the lateral control demand filter cascades described in Section IV.D are replaced by the filter method presented below. To simplify the discussion of the algorithm, e is used to denote the lateral displacement demand and the $*$ is omitted since all processed variables are demands.

In the first step of the filter algorithm the lateral displacement demand e is saturated by $\underline{e}$ and $\bar{e}$ based on the curvature limits of the vehicle $\bar{\kappa}$ and $\underline{\kappa}$, discussed in Section V.D, and the maximum demanded path curvature $\hat{\kappa}_{\mathrm{P}}$ within a speed dependent window ahead of the current position

$$\underline{e} = \frac{1}{\bar{\kappa}} - \frac{1}{\hat{\kappa}_{\mathrm{P}}} \qquad (35) \qquad \bar{e} = \frac{1}{\underline{\kappa}} - \frac{1}{\hat{\kappa}_{\mathrm{P}}}. \qquad (36)$$

Based on the saturated demand value e_{sat} the lateral displacement rate demand $\frac{\mathrm{d}e}{\mathrm{d}q}$ is calculated according to filter equation (31).

Next an approximate solution of (22) is used for the limit calculation of $\frac{\mathrm{d}e}{\mathrm{d}q}$ and $\Delta\psi$. Based on the assumptions that the lateral displacement control error $e_y^{\mathrm{P}^*} - e_y^{\mathrm{P}}$ and the tangential displacement e_x^{P} are both zero the following approximation is used

$$\beta = -\operatorname{asin}\left(\frac{\mathrm{d}e}{\mathrm{d}q}\right) + \Delta\psi. \qquad (37)$$

Starting from this relation the limits of the orientation offset $\Delta\bar{\psi}$ and $\Delta\underline{\psi}$ are expressed in (38) and (39) considering the side slip angle limits $\underline{\beta}(\kappa_{\mathrm{C}})$ and $\bar{\beta}(\kappa_{\mathrm{C}})$, introduced in Section V.D, the current curvature of the vehicle path κ_{C} and the lateral displacement rate demand $\frac{\mathrm{d}e}{\mathrm{d}q}$

$$\Delta\underline{\psi} = \underline{\beta}(\kappa_{\mathrm{C}}) + \operatorname{asin}\left(\frac{\mathrm{d}e}{\mathrm{d}q}\right) \qquad (38)$$

$$\Delta\bar{\psi} = \bar{\beta}(\kappa_{\mathrm{C}}) + \operatorname{asin}\left(\frac{\mathrm{d}e}{\mathrm{d}q}\right). \qquad (39)$$

The curvature of the actual vehicle path is estimated using the lateral displacement demand of the previous time step e_{pre} and the curvature of the demanded path at the current position κ_{P}

$$\kappa_{\mathrm{C}} = \frac{\kappa_{\mathrm{P}}}{1 + \kappa_{\mathrm{P}} \cdot e_{\mathrm{pre}}}. \qquad (40)$$

Next the orientation offset $\Delta\psi$ is saturated to its limits and subsequently filtered using (32). Following this, the limits of the feasible lateral displacement rate demand $\frac{\mathrm{d}\bar{e}}{\mathrm{d}q}$ and $\frac{\mathrm{d}e}{\mathrm{d}q}$ are calculated using the same approach as for the $\Delta\psi$ limits. Substituting the filtered orientation offset demand $\Delta\psi_{\mathrm{filt}}$ and the side slip angle limits $\underline{\beta}(\kappa_{\mathrm{C}})$ and $\bar{\beta}(\kappa_{\mathrm{C}})$ into (37) yields

$$\frac{\mathrm{d}e}{\mathrm{d}q} = \sin\left(\Delta\psi_{\mathrm{filt}} - \bar{\beta}(\kappa_{\mathrm{C}})\right) \tag{41}$$

$$\frac{\mathrm{d}\bar{e}}{\mathrm{d}q} = \sin\left(\Delta\psi_{\mathrm{filt}} - \underline{\beta}(\kappa_{\mathrm{C}})\right). \tag{42}$$

Finally, the lateral displacement rate demand is saturated and the filtered lateral displacement demand e_{filt} is calculated using the rate limited filter (33).

The key element of the presented supervisor method is the geometric vehicle model used to represent the steering angle limits in form of curvature and side slip angle limits. The derivation of these limits is discussed in the next section.

D. Vehicle curvature and side slip angle limit calculation

Assuming that the vehicle is following its path with zero tire slip, the steering angles of two wheels define the ICR as illustrated in Fig. 4. Based on the position of the ICR relative to the vehicle center, the relationship between vehicle path curvature κ_{C} and the side slip angle β can be derived.

Using this geometric relation the maximum (minimum) curvature results from the maximum (minimum) front steering angle δ_i and the minimum (maximum) rear steering angle δ_k of the left (right) vehicle half.

Deriving the side slip angle limits, β is expressed in dependence of the curvature κ_{C}, the wheel hub position of tire j and the respective steering angle δ_j. The resulting functions $\beta_j(\kappa_{\mathrm{C}}, \delta_j)$ are monotonically increasing in δ_j and define feasible side slip regions. Each region considers the steering angle constraints of tire j. The region respecting the constraints of all steering angles results from the intersection of these regions. The considered regions are one-dimensional and connected such that the intersection is constrained by the minimum upper bound and the maximum lower bound

$$\bar{\beta}(\kappa_{\mathrm{C}}) = \min_{j\in\{1\ldots4\}} \bar{\beta}_j\,(\kappa_{\mathrm{C}}, \delta_j) \tag{43}$$

$$\underline{\beta}(\kappa_{\mathrm{C}}) = \max_{j\in\{1\ldots4\}} \underline{\beta}_j(\kappa_{\mathrm{C}}, \delta_j). \tag{44}$$

VI. Evaluation and Experimental Results

In the final section of this paper the performance of the proposed supervised geoPFC is presented. First the capabilities of the demand supervisor are demonstrated in a simulation. Secondly results from a test drive with the complete control system implemented on the ROboMObil are shown.

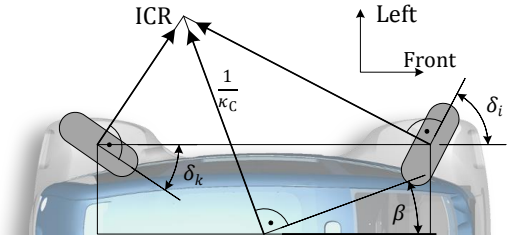

Fig. 4: Geometrical model used for curvature and side slip angle limit calculation.

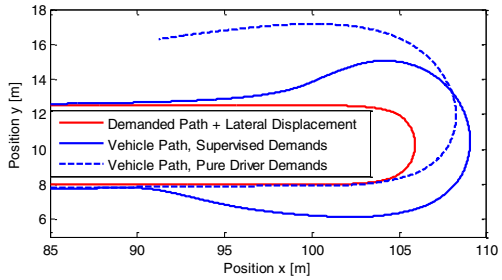

Fig. 5: Comparison of the simulation results for the path following capabilities of the geoPFC with and without driver demand supervisor. The plot shows the same time window for both simulations.

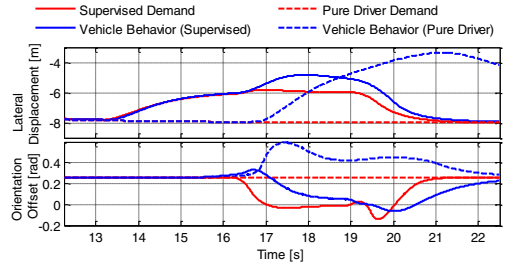

Fig. 6: Comparison of the simulated demad progress and control accuracy of the geoPFC with and without driver demand supervisor.

A. Evaluation of demand supervisor

The evaluation scenario presented is a U-Turn with lateral displacement demand, the red line in Fig. 5, resulting in a demanded curve radius of two meters. This is lower than the theoretical limit of 3.3 m feasible with the maximum steering angles of 25°. In addition to the high curvature an orientation offset of 15° is demanded in the test maneuver. This test has been simulated for the geoPFC with and without the supervisor. In Fig. 5 and Fig. 6 the resulting demand and vehicle behavior is illustrated for both cases. Fig. 5 shows that in the supervised case the vehicle reacts in advance to avoid infeasible curvature demands, whereas in the unsupervised case the vehicle drifts off in the corner and hence needs longer to return to the demanded path. Fig. 6 shows that the supervisor additionally reduces the orientation offset demand to lower the steering angle bias limiting the geoPFC actions. Furthermore it shows that the difference between demanded and vehicle behavior is reduced when the supervisor is active. Altogether these results show that the demand supervisor significantly improves the path following behavior in case of infeasible driver demands.

B. Experimental validation

For the experimental validation of the supervised geoPFC, the presented algorithm has been implemented on a Rapid Control Prototyping Platform in the ROboMObil and a dGPS-aided inertial navigation system is used to generate the control feedback. Various tests have been performed to tune the setup and check the reliability and safety of the supervised geoPFC. After concluding these tests the controller has been tested by unexperienced ROboMObil

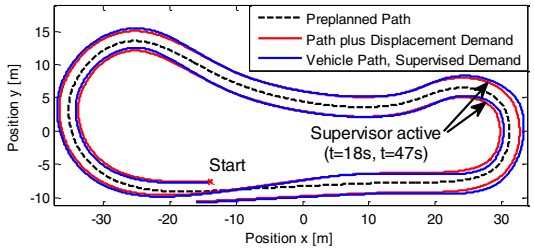

Fig. 7: Measurements from a guest drive showing the path following capabilities of the geoPFC with driver demand supervisor.

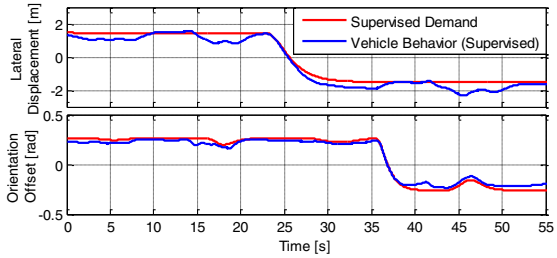

Fig. 8: Measured demand progress and vehicle response from a guest drive showing the achieved control accuracy of the geoPFC with activated driver demand supervisor.

drivers in geoPFC mode. In Fig. 7 the test course is illustrated as black dashed line. In Fig. 7 and Fig. 8 the supervised driver demand in red and the measured vehicle path in blue depict two laps of the test session. Although the test course is not as demanding as the simulated validation course in Fig. 5, Fig. 8 shows a slight modification of the orientation offset at time 18 s and 47 s by the demand supervisor. Overall the results here represent the good tracking behavior of the geoPFC and the reliability of the supervisor observed in the test drives.

VII. Conclusion And Outlook

The presented work combines a time independent formulation of a path following controller with a demand supervisor based on a geometric vehicle model able to reduce commanded lateral demands to maintain the feasibility of the path following task. The derived geoPFC with its speed normalized interface to the GCA is feasible for all vehicle speeds, especially for zero speed. This compensates the major drawback of the time independent PFC adapted to the GCA in an early stage of this work. The proposed algorithm enables the tracking of predefined paths, with high accuracy and assures the stability of the vehicle even in situations where the vehicle is at its limits and an unsupervised demand would lead to instability.

The framework has been extensively tested by various drivers in real world test drives with the ROboMObil and performed well. In future studies the geoPFC can be used as a service provided by the ROboMObil. For example is it used in a platooning application and helps to generate reproducible vehicle dynamics test data in an automatic test drive service.

Acknowledgment

The authors express their gratitude to the ROboMObil team and the head of the institute Johann Bals for their support.

References

[1] J. Brembeck, L. M. Ho, A. Schaub, C. Satzger and G. Hirzinger, "Romo - The robotic electric Vehicle," in *22nd International Symposium on Dynamics of Vehicle on Roads and Tracks*, 2011.

[2] J. Ziegler, P. Bender, M. Schreiber, H. Lategahn, T. Strauss, C. Stiller, T. Dang, U. Franke, N. Appenrodt, C. Keller, E. Kaus, R. Herrtwich, C. Rabe, D. Pfeiffer, F. Lindner, F. Stein, F. Erbs, M. Enzweiler, C. Knöppel, J. Hipp, M. Haueis, M. Trepte, C. Brenk, A. Tamke, M. Ghanaat, M. Braun, A. Joos, H. Fritz, H. Mock, M. Hein and E. Zeeb, "Making Bertha Drive—An Autonomous Journey on a Historic Route," *IEEE Intelligent Transportation Systems Magazine,* pp. 8-20, 7 2014.

[3] H. Fritz, A. Gern, H. Schiemenz and C. Bonnet, "CHAUFFEUR Assistant: a driver assistance system for commercial vehicles based on fusion of advanced ACC and lane keeping," in *IEEE Intelligent Vehicles Symposium*, Parma, 2004.

[4] J. Bohren, T. Foote, J. Keller, A. Kushleyev, D. Lee, A. Stewart, P. Vernaza, J. Derenick, J. Spletzer and B. Satterfield, "Little Ben: The Ben Franklin Racing Team's entry in the 2007 DARPA Urban Challenge," *Journal of Field Robotics,* no. 25, p. 598–614, 2008.

[5] J. Ziegler, M. Werling and J. Schroder, "Navigating car-like robots in unstructured environments using an obstacle sensitive cost function," in *IEEE Intelligent Vehicles Symposium*, Eindhoven, 2008.

[6] P. Ritzer, C. Winter and J. Brembeck, "Advanced path following control of an overactuated robotic vehicle," in *IEEE Intelligent Vehicles Symposium*, Seoul, 2015.

[7] T. Buente, J. Brembeck and L. M. Ho, "Human machine interface concept for interactive motion control of a highly maneuverable robotic vehicle," in *Intelligent Vehicle Symposium*, Baden-Baden, 2011.

[8] R. de Castro, T. Bünte and J. Brembeck, "Design and Validation of the Second Generation of the Robomobil's Vehicle Dynamics Controller," in *International Symposium on Dynamics of Vehicles on Roads and Tracks (IAVSD)*, Graz, 2015.

[9] J. Brembeck and C. Winter, "Real-time capable path planning for energy management systems in future vehicle architectures," in *IEEE Intelligent Vehicles Symposium Proceedings*, 2014.

[10] M. Sampei, "A Control Strategy for a Class of Non-Holonomic Systems - Time-State Control Form and its Application," in *Conference on Decision and Control*, Lake Buena Vista, 1994.

[11] E. Johnson and A. Calise, "Limited Authority Adaptive Flight Control for Reusable Launch Vehicles," *Journal of Guidance, Control and Dynamics,* vol. 26, no. 6, 2003.